

THE SINS/ZC-SINF SURVEY OF $z \sim 2$ GALAXY KINEMATICS: OUTFLOW PROPERTIES*

SARAH F. NEWMAN^{1,16}, REINHARD GENZEL^{1,2,3}, NATASCHA M. FÖRSTER-SCHREIBER², KRISTEN SHAPIRO GRIFFIN⁴, CHIARA MANCINI⁷, SIMON J. LILLY⁶, ALVIO RENZINI⁷, NICOLAS BOUCHE^{8,9}, ANDREAS BURKERT¹⁰, PETER BUSCHKAMP², C. MARCELLA CAROLLO⁶, GIOVANNI CRESCI¹¹, RIC DAVIES², FRANK EISENHAUER², SHY GENEL⁵, ERIN K. S. HICKS¹², JARON KURK², DIETER LUTZ², THORSTEN NAAB¹³, YINGJIE PENG⁶, AMIEL STERNBERG¹⁴, LINDA J. TACCONI², DANIELA VERGANI¹⁵, STIJN WUYTS², AND GIANNI ZAMORANI¹⁵

Draft version February 19, 2018

ABSTRACT

Using SINFONI H α , [NII] and [SII] AO data of 27 $z \sim 2$ star-forming galaxies (SFGs) from the SINS and zC-SINF surveys, we explore the dependence of outflow strength (via the broad flux fraction) on various galaxy parameters. For galaxies that have evidence for strong outflows, we find that the broad emission is spatially extended to at least the half-light radius (\sim a few kpc). Decomposition of the [SII] doublet into broad and narrow components suggests that this outflowing gas probably has a density of ~ 10 – 100 cm⁻³, less than that of the star forming gas (600 cm⁻³). There is a strong correlation of the H α broad flux fraction with the star formation surface density of the galaxy, with an apparent threshold for strong outflows occurring at 1 M $_{\odot}$ yr⁻¹ kpc⁻². Above this threshold, we find that SFGs with $\log m_{*} > 10$ have similar or perhaps greater wind mass loading factors ($\eta = \dot{M}_{\text{out}}/\text{SFR}$) and faster outflow velocities than lower mass SFGs, suggesting that the majority of outflowing gas at $z \sim 2$ may derive from high-mass SFGs. The mass loading factor is also correlated with the SFR, galaxy size and inclination, such that smaller, more star-forming and face-on galaxies launch more powerful outflows. We propose that the observed threshold for strong outflows and the observed mass loading of these winds can be explained by a simple model wherein break-out of winds is governed by pressure balance in the disk.

Subject headings: cosmology: observations — galaxies: high-redshift — galaxies: evolution — infrared: galaxies

1. INTRODUCTION

* Based on observations at the Very Large Telescope (VLT) of the European Southern Observatory (ESO), Paranal, Chile (ESO program IDs 076.A-0527, 079.A-0341, 080.A-0330, 080.A-0339, 080.A-0635, 183.A-0781).

¹ Department of Astronomy, Campbell Hall, University of California, Berkeley, CA 94720, USA

² Max-Planck-Institut für extraterrestrische Physik (MPE), Giessenbachstr.1, D-85748 Garching, Germany

³ Department of Physics, Le Conte Hall, University of California, Berkeley, CA 94720, USA

⁴ Space Sciences Research Group, Northrop Grumman Aerospace Systems, Redondo Beach, CA 90278, USA

⁵ Harvard-Smithsonian Center for Astrophysics, 60 Garden Street, Cambridge, MA 02138 USA

⁶ Institute of Astronomy, Department of Physics, Eidgenössische Technische Hochschule, ETH Zürich, CH-8093, Switzerland

⁷ Osservatorio Astronomico di Padova, Vicolo dell'Osservatorio 5, Padova, I-35122, Italy

⁸ Université de Toulouse; UPS-OMP; IRAP; Toulouse, France

⁹ CNRS; IRAP; 14, avenue Edouard Belin, F-31400 Toulouse, France

¹⁰ Universitäts-Sternwarte Ludwig-Maximilians-Universität (USM), Scheinerstr. 1, München, D-81679, Germany

¹¹ Istituto Nazionale di Astrofisica Osservatorio Astronomico di Arcetri, Largo Enrico Fermi 5, I 50125 Firenze, Italy

¹² Department of Astronomy, University of Washington, Box 351580, U.W., Seattle, WA 98195-1580, USA

¹³ Max-Planck Institute for Astrophysics, Karl Schwarzschildstrasse 1, D-85748 Garching, Germany

¹⁴ INAF Osservatorio Astronomico di Bologna, Via Ranzani 1, 40127 Bologna, Italy

¹⁵ School of Physics and Astronomy, Tel Aviv University, Tel Aviv 69978, Israel

¹⁶ email: sfnewman@berkeley.edu

Most high- z SFGs from rest-UV/optical samples show evidence for powerful galactic outflows, as indicated by UV absorption spectroscopy (Pettini et al. 2000; Shapley et al. 2003; Steidel et al. 2010; Weiner et al. 2009; Kornei et al. 2012) and broad H α emission-line profiles (Shapiro et al. 2009; Genzel et al. 2011; Newman et al. 2012). This ‘star formation feedback’ may be an essential ingredient in the evolution of high- z star forming galaxies, particularly between $z \sim 1$ – 3 , at the peak of the star formation rate density (Hopkins & Beacom 2006). However, little is yet known about how galaxy parameters determine the prevalence and strength of these outflows.

Current theoretical models suggest that outflows could be driven by energy or momentum feedback (e.g. Murray et al. 2005). In the simple momentum driven wind scenario of Oppenheimer & Davé (2006, 2008), the mass loading parameter of the wind primarily depends on the circular velocity of the disk v_d , $\eta \propto v_d^{-1} \propto M_{\text{baryon}}^{-1/3}$, if the wind outflow velocity is near the escape velocity (Murray et al. 2005). Hopkins et al. (2012) have recently carried out high-resolution SPH simulations of isolated galaxies with different types of input feedback, including that from supernovae, stellar winds, expanding HII regions and radiation pressure and find an overall scaling of $\eta \propto v_d^{-1} \Sigma_{\text{gas}}^{-1/2}$ and $\eta \sim 1$ for the parameters of typical high- z massive SFGs and with energy-driven winds. The scaling with v_d^{-1} is consistent with that found by Oppenheimer & Davé (2006, 2008), yet the dependence

on $\Sigma_{gas}^{-1/2}$ is contrary to the findings of Chen et al. (2010), who found a positive correlation of Na D equivalent width (EW) with Σ_{SFR} from SDSS data of $\sim 100,000$ galaxies, where Na D EW is used here as a proxy for the mass loading (η).

In this paper we analyze the outflow properties of 27 $z \sim 2$ SFGs, discussed in more detail in Förster Schreiber et al. (2012) and based on new high-quality H α emission line SINFONI/VLT integral field (IFU) spectroscopy with adaptive optics (AO) (Eisenhauer et al. 2003; Bonnet et al. 2004). We adopt a Λ CDM cosmology with $\Omega_m = 0.27$, $\Omega_b = 0.046$ and $H_0 = 70$ km/s/Mpc (Komatsu et al. 2011), and a Chabrier (2003) initial stellar mass function (IMF).

2. OBSERVATIONS, DATA REDUCTION AND ANALYSIS TECHNIQUES

The galaxy sample discussed here (see Table 1) is described in Mancini et al. (2011); Förster Schreiber et al. (2012). Our 27 $z \sim 2$ –2.5 SFGs are drawn from the SINS and zC-SINF surveys of H α + [NII] integral field spectroscopy with SINFONI on the ESO VLT (Förster Schreiber et al. 2009; Mancini et al. 2011; Förster Schreiber et al. 2012). They were selected either from their U_n GR colors satisfying the ‘BX’ criteria (Steidel et al. 2004; Adelberger et al. 2004; Erb et al. 2006; Law et al. 2009) or based on K band imaging via the ‘BzK’ criterion for $1.4 < z < 2.5$ SFGs (Daddi et al. 2004). They sample the $z \sim 2.2$ star-forming ‘main sequence’ for stellar masses between $10^{9.5}$ to $10^{11.5} M_\odot$. Our sample includes 25 galaxies observed with AO-mode with sufficient SNR for analysis (0.05” pixels, typical FWHM 0.2–0.25”) in addition to 2 galaxies observed in seeing limited mode that have very extended disks and thus are well resolved with 0.125” pixels and FWHM ~ 0.5 ”. The data are of high quality (~ 6 h average integration time per galaxy, with a range from 2 to 22h, and a total integration time for the entire sample of 180h) and were reduced with our standard data reduction methods and analysis tools (Schreiber et al. 2004; Davies 2007; Förster Schreiber et al. 2009; Mancini et al. 2011).

Stellar masses and ages are derived from SED modeling in Förster Schreiber et al. (2009); Mancini et al. (2011) assuming constant or exponentially declining star formation histories with Bruzual & Charlot (2003) tracks. The SFRs are derived from the SED modeling and from H α ($SFR = L_{H\alpha} / 2.1 \times 10^{41}$ erg/s, Kennicutt (1998), corrected for a Chabrier (2003) IMF) with a Calzetti et al. (2000) reddening law with $A_{V,gas} = 2.3 \times A_{V,SED}$. Half light radii ($R_{1/2}$) were computed from the cumulative H α flux profile determined after fitting a 2D exponential (Sersic $n = 1$) to the data. We calculate molecular gas masses (M_{gas}) and surface densities ($\Sigma_{gas} = 0.5 \times M_{gas} / (\pi R_{1/2}^2)$) from the H α -derived SFRs using the molecular gas to star formation surface density relation with $M_{gas}(M_\odot) = 5.8 \times 10^8 \times SFR (M_\odot yr^{-1})$ (Tacconi et al. 2012).

To isolate the broad emission for coadding, we remove large-scale rotational velocity gradients from the data cubes by aligning the spectral axis of each pixel, such that the H α peak lies at the same velocity throughout the cube. This technique minimizes the width of the galaxy integrated spectrum due to large scale motions (e.g. ro-

TABLE 1
GALAXY PROPERTIES

Galaxy ID	Reference	m_* ($10^{11} M_\odot$)	SFR (H α) (M_\odot/yr)	Σ_{SFR} ($M_\odot yr^{-1} kpc^{-2}$)
Q1623-BX455	1,2	0.10 ± 0.031	63 ± 19	1.66 ± 0.52
Q1623-BX502	1,2	0.023 ± 0.0070	40 ± 12	2.86 ± 0.90
Q1623-BX543	1,2	0.094 ± 0.028	183 ± 55	2.38 ± 0.98
Q1623-BX599	1,2	0.57 ± 0.17	131 ± 39	3.95 ± 1.63
SSA22a-MD41	1,2,3	0.077 ± 0.010	131 ± 39	0.80 ± 0.24
Q2343-BX389	1,2	0.41 ± 0.080	196 ± 59	0.74 ± 0.22
Q2343-BX513	1,2	0.27 ± 0.081	28 ± 8	1.00 ± 0.36
Q2343-BX610	1,2	1.00 ± 0.27	212 ± 64	1.15 ± 0.35
Q2343-BX482	1,2	0.18 ± 0.080	121 ± 36	0.61 ± 0.19
GMASS-2303	4	0.072 ± 0.022	30 ± 9	0.52 ± 0.16
GMASS-2363	4	0.22 ± 0.065	50 ± 15	1.17 ± 0.37
ZC-401925	5,6,7	0.052 ± 0.016	13 ± 4	0.19 ± 0.060
ZC-404221	5,6,7	0.11 ± 0.050	60 ± 18	1.80 ± 0.57
ZC-405501	5,6,7	0.10 ± 0.030	68 ± 20	0.26 ± 0.10
ZC-405226	5,6,7	0.092 ± 0.028	82 ± 25	0.34 ± 0.17
ZC-406690	5,6,7	0.44 ± 0.13	480 ± 144	1.87 ± 0.57
ZC-407376	5,6,7	0.20 ± 0.060	283 ± 85	2.43 ± 0.77
ZC-407302	5,6,7	0.30 ± 0.090	260 ± 78	2.72 ± 0.83
ZC-409985	5,6,7	0.12 ± 0.036	40 ± 12	0.81 ± 0.25
ZC-410041	5,6,7	0.042 ± 0.013	105 ± 31	0.72 ± 0.22
ZC-410123	5,6,7	0.042 ± 0.013	40 ± 12	0.30 ± 0.090
ZC-411737	5,6,7	0.040 ± 0.015	60 ± 18	1.06 ± 0.33
ZC-412369	5,6,7	0.18 ± 0.050	182 ± 55	1.72 ± 0.60
ZC-413507	5,6,7	0.088 ± 0.025	92 ± 28	1.19 ± 0.43
ZC-413597	5,6,7	0.070 ± 0.020	86 ± 26	1.72 ± 0.55
ZC-415876	5,6,7	0.084 ± 0.022	42 ± 13	2.33 ± 0.80
SA12-6339	5,6,7	0.26 ± 0.077	681 ± 204	17.34 ± 9.41

References for parent sample. (1) Erb et al. (2006), (2) Steidel et al. (2004), (3) Erb et al. (2003), (4) Kurk et al. (2009), (5) Lilly et al. (2007), (6) Lilly et al. (2009), (7) McCracken et al. (2010).

tation) in the narrow velocity component, and thus maximizes the contrast between the broad and narrow components. Shapiro et al. (2009) demonstrated that this method does not create artificial broad wings. From these velocity-shifted data cubes, we create spatially-integrated spectra for each galaxy by collapsing the cubes onto a single spectral axis (see: Förster Schreiber et al. 2009; Shapiro et al. 2009). Various stacks of spectra are generated by removing a fitted continuum from each spectrum, placing the spectra on a common rest-frame wavelength axis, weighting each spectrum by the signal to noise ratio (SNR) of H α , and coadding the final spectra.

Broad emission has previously been detected in SINS/zC-SINF galaxies by Shapiro et al. (2009); Genzel et al. (2011); Newman et al. (2012) and attributed to galactic outflows. We quantify the fraction of the emission line flux in this underlying broad component by simultaneously fitting two Gaussian functions to each of the H α , [NII] $\lambda\lambda 6548, 6584$ and [SII] $\lambda\lambda 6716, 6731$ emission lines, setting the kinematics (velocity, line width) of all of the narrow Gaussian components to be equal to each other, and likewise setting the kinematics of the broad Gaussian components equal to each other. We allow the broad H α flux to vary, but set the [NII]/H α ratio in the broad component to the [NII]/H α ratio in the narrow component (and likewise for [SII]/H α). Genzel et al. (2011) demonstrated that in the absence of a broad component, and after removal of large scale velocity shifts as described above, the remaining velocity profiles can be well fit by Gaussians. The ‘broad flux fraction’ is defined as the ratio of the flux in the broad

H α emission line to the flux in the narrow H α emission line.

We also generate position-velocity (pv) data by extracting the spectra along the major galaxy axis for each shifted cube with a slit wide enough to cover most of the minor axis emission. The data are then co-added and re-sampled onto a normalized spatial scale of $0.07 \times R_{1/2}$ (FWHM $\sim 0.3 \times R_{1/2}$) and spectral scale of 40 km/s/pixel (~ 90 km/s FWHM).

3. OUTFLOW PROPERTIES IN $z \sim 2$ SFGS

We ascertain that the outflows are driven by the star formation activity and not by an AGN as we have excluded any known AGN from our sample, find that the broad emission is extended and not concentrated towards the kinematic or morphological center (see section 3.1), and measure [NII]/H α ratios compatible with the expected metallicity based on the $z \sim 2$ mass-metallicity relation (Erb et al. 2006) and too low to be consistent with the presence of an AGN. In two cases we trace the origin of the outflows to individual giant star forming clumps embedded in the disk (Genzel et al. 2011; Newman et al. 2012). We note that Genzel et al. (2011) suggest that the bright emission coming from a clump in one of our galaxies (ZC407302) could be due to AGN activity if this clump is an external minor merger, rather than a star forming clump formed within the disk. However, there is no other evidence that this galaxy contains an AGN.

3.1. Outflows are Spatially Extended

The broad emission (FWHM ~ 450 km/s) is spatially extended over the half-light radii ($R_{1/2}$), which corresponds to a few kpc in the small galaxies and up to 6 kpc in the larger disks. This is demonstrated in the bottom panel of Figure 1, where we show a co-added pv diagram of the line emission (large-scale velocity gradients removed) along the morphological major axis for the galaxies. Broad emission is detected at least out to $R_{1/2}$, and its width between $0.5 \times R_{1/2}$ and $R_{1/2}$ (FWHM = 423 ± 19 km/s) is nearly as broad as within $0.5 \times R_{1/2}$ (FWHM = 475 ± 12 km/s). The upper panel of Figure 1 shows that the emission in the outer regions of the galaxies is almost as broad as in the inner regions, and implies a constant or decreasing mass-loading with increasing galacto-centric radius.

The 10 galaxies used in this coadd (BX455, BX513, BX543, BX599, SA12-6339, ZC404221, ZC407306, ZC407302, ZC412369, ZC415876) are selected such that they have noticeable broad line wings without the need for stacking and an absence of OH residuals near H α . All but one have $R_{1/2} < 3$ kpc and all have $\Sigma_{SFR} > 1 M_{\odot} yr^{-1} kpc^{-2}$. However, their stellar masses and SFRs span the ranges seen in our full sample. We note that although most of the galaxies from this stack are small (with $R_{1/2} < 3$ kpc), we also observe broad emission from stacks of larger galaxies that also have $\Sigma_{SFR} > 1 M_{\odot} yr^{-1} kpc^{-2}$ (see next section).

3.2. The Broad Flux Fraction is Strongly Dependent on the SF Surface Density

We explore the dependence of the broad flux fraction on galaxy properties by dividing the entire sample into

two bins each (low/high) in star formation rate, stellar mass, size, inclination and star formation surface density. We then co-added the spectra in each of the bins and computed the ratio of the broad to narrow H α emission. The results are summarized in Table 2.

The star formation surface density has the largest effect on the broad flux fraction, such that galaxies with $\Sigma_{SFR} > 1 M_{\odot} yr^{-1} kpc^{-2}$ drive the strongest outflows, which confirms and strengthens a similar finding in Genzel et al. (2011). This result is also consistent with what was observed in $z \sim 0$ SFGs by Chen et al. (2010), where they found a strong correlation of Na D absorption equivalent width (from SDSS data of $\sim 100,000$ galaxies) with Σ_{SFR} .

In Figure 2, we see the dependence of the broad H α flux fraction on Σ_{SFR} from 5 Σ_{SFR} -binned points as well as three massive star-forming clumps. The trend seen in Figure 2 can be well described as a ‘threshold’ for outflows. All of the data points with $\Sigma_{SFR} > 1 M_{\odot} yr^{-1} kpc^{-2}$ have $F_{broad}/F_{narrow} > 0.7$, while all those below this threshold have $F_{broad}/F_{narrow} \leq 0.25$. We also compare the spectra and broad component fits for stacks of galaxies above and below the Σ_{SFR} threshold in the lower panels of Figure 2. For these high Σ_{SFR} and low Σ_{SFR} stacks, the two-component fits yield a reduced χ^2 of 1.15 and 1.55, respectively, while an imposed single-component fit yields reduced χ^2 values of 16.9 and 3.27, indicating that a two-component fit is much better in the stack with a higher F_{broad}/F_{narrow} ratio, and thus stronger wind signature, and somewhat better in the stack with a smaller outflow signature.

The broad flux fraction also varies (to a lesser extent) with m_* , SFR, $R_{1/2}$ and inclination such that higher F_{broad}/F_{narrow} values and thus stronger outflows are observed for massive, high SFR, compact, face-on galaxies. We further explore the m_* trend by dividing each of the high and low Σ_{SFR} bins into high and low m_* bins. Unsurprisingly, we find that both of the m_* bins below this threshold show negligible evidence for broad emission, and both high Σ_{SFR} bins show strong outflows. Above the Σ_{SFR} threshold, the broad flux fraction is similar or perhaps somewhat larger in the high m_* bin. The FWHM of the broad line is larger for the high m_* bin (520 ± 11 km/s vs. 428 ± 30 km/s) and more blueshifted (-25 ± 4 km/s vs. -13 ± 7 km/s). This increase is smaller than a ‘virial’ scaling, $v_{out} \leq v_{esc} \sim v_c \sim m_*^{0.33}$ (Murray et al. 2005; Martin 2005), which would imply a factor of ~ 1.8 in v_{out} between the two mass bins ($\log m_* = 9.85$ and 10.61).

The SFR trend is linked to that of m_* , due to the strong correlation of m_* and SFR for ‘main-sequence’ SFGs at all redshifts. The $R_{1/2}$ trend is likely due to the higher Σ_{SFR} values for the more compact galaxies. The trend with inclination supports a bipolar outflow emerging perpendicularly from the plane of the star-forming disk, consistent with the results of Kornei et al. (2012, at $z \sim 1$), Chen et al. (2010, at $z \sim 0$), Bouché et al. (2012) and Bordoloi et al. (2011) (but see Law et al. (2012)).

3.3. Local Electron Density of the Outflow

We estimate the ratio of the [SII] doublet in the broad and narrow components for a stack of the galaxy spectra, in order to constrain the star-forming gas and wind

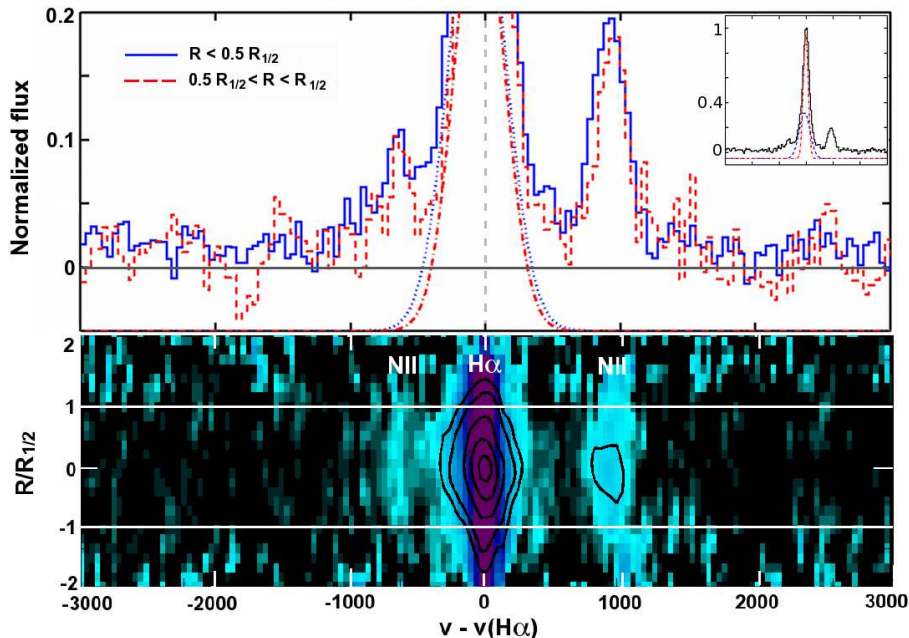


FIG. 1.— Lower panel: Co-added (pv) diagram for the 10 sources with the best evidence for broad emission, with the vertical (spatial) axis normalized to $R_{1/2}$. The black contours show the unnormalized stack, while the colors have been normalized according to the peak $H\alpha$ flux for each spatial row. The broad emission in light blue (>200 – 300 km/s from the systemic velocity) is spatially extended (vertical axis) out to at least $R_{1/2}$. Upper panel: Spectra from the inner ($R < 0.5 \times R_{1/2}$, blue, solid line) and outer ($0.5 \times R_{1/2} < R < R_{1/2}$, red, dashed line) regions of the galaxies, with the broad fitted components shown by the blue dotted line (inner) and red dash-dotted line (outer). The inner and outer region spectra have $F_{broad}/F_{narrow} = 1.31 \pm 0.075$ and 1.13 ± 0.12 with broad to narrow component velocity shifts of -41 ± 5 km/s and -33 ± 9 km/s, respectively. The inset shows the entire $H\alpha$ line for the inner spectrum (black) with the broad component (blue, dashed) and narrow component (red, dash-dot) overlaid.

TABLE 2
BROAD FLUX FRACTION FOR HIGH AND LOW BINS OF DIFFERENT GALAXY PROPERTIES

Property	F_{broad}/F_{narrow} ($H\alpha$)		FWHM _{broad} (km/s)		$\Delta v_{broad-narrow}$ (km/s)		Significance of difference	Dividing value
	High bin	Low bin	High bin	Low bin	High bin	Low bin		
SFR	0.65 ± 0.074	0.50 ± 0.041	510 ± 12	423 ± 47	-23 ± 4	-21 ± 8	2σ	$100 M_{\odot}/\text{yr}$
$R_{1/2}$	0.50 ± 0.054	0.76 ± 0.082	503 ± 15	432 ± 19	-15 ± 6	-35 ± 6	3σ	3 kpc
Σ_{SFR}	0.77 ± 0.027	0.16 ± 0.030	500 ± 16	423 ± 75	-27 ± 4	-43 ± 23	20σ	$1 M_{\odot} \text{yr}^{-1} \text{kpc}^{-2}$
inclination	0.47 ± 0.055	0.77 ± 0.091	510 ± 44	514 ± 12	-39 ± 14	-32 ± 5	3σ	49 – 55°
m_{*}^1	0.63 ± 0.056	0.41 ± 0.042	528 ± 13	423 ± 45	-32 ± 5	-20 ± 8	4σ	$1 \times 10^{10} M_{\odot}$
m_{*}^2	0.23 ± 0.21	0.12 ± 0.040	423 ± 66	423 ± 80	-28 ± 18	-48 ± 42	0.5σ	"
m_{*}^3	0.85 ± 0.097	0.71 ± 0.10	520 ± 11	428 ± 30	-25 ± 4	-13 ± 7	1.5σ	"

The high/low bins for SFR, m_{*} , Σ_{SFR} , $R_{1/2}$, and inclination are divided above and below the value(s) shown in column 9 and have roughly an equal number of galaxies in each bin. The spectrum from each stack was fit constraining the narrow FWHM to between 190 and 210 km/s, so that the broad component was not fit as a very broad narrow component, and allowing the relative velocities of the two components and the broad line width (FWHM) to vary. The best fit broad FWHM and the relative velocities for each bin are shown in columns 4–7. For the m_{*} bins, (1) is for all galaxies, (2) is for galaxies with $\Sigma_{SFR} < 1 M_{\odot} \text{yr}^{-1} \text{kpc}^{-2}$, and (3) is for galaxies with $\Sigma_{SFR} > 1 M_{\odot} \text{yr}^{-1} \text{kpc}^{-2}$.

densities. The 14 galaxies used in this stack are selected such that they do not have strong OH sky features close to the location of the [SII] lines and have noticeable broad $H\alpha$ components. We follow the fitting method described earlier in the text, except here we allow the amplitudes of the broad and narrow components in all nebular lines to vary, as opposed to, for instance, setting [NII]/ $H\alpha$ (broad) equal to [NII]/ $H\alpha$ (narrow). The reduced χ^2 of the fit in the region of the $H\alpha$ line is 1.71 and in the region of the [SII] lines is 0.97, while an imposed one-component fit yields reduced χ^2 values of 26.1 and 1.24, respectively, highlighting the challenges of attempting such a measure-

ment.

For the narrow component, we find $F([\text{SII}]\lambda 6716)/F([\text{SII}]\lambda 6731) = 0.99 \pm 0.27$, and for the broad component, we find that the ratio = 1.43 ± 0.40 , corresponding to electron densities of 600 (+1000/-450) and 10 (+590/-10) cm^{-3} , respectively (Osterbrock 1989). The errors come from the fit uncertainties. Although our estimate is uncertain, the inferred local gas density in the outflow could be more than an order of magnitude less than the density of the star-forming regions (traced by the narrow component), consistent with a diffuse outflow. In Newman et al. (2012), we

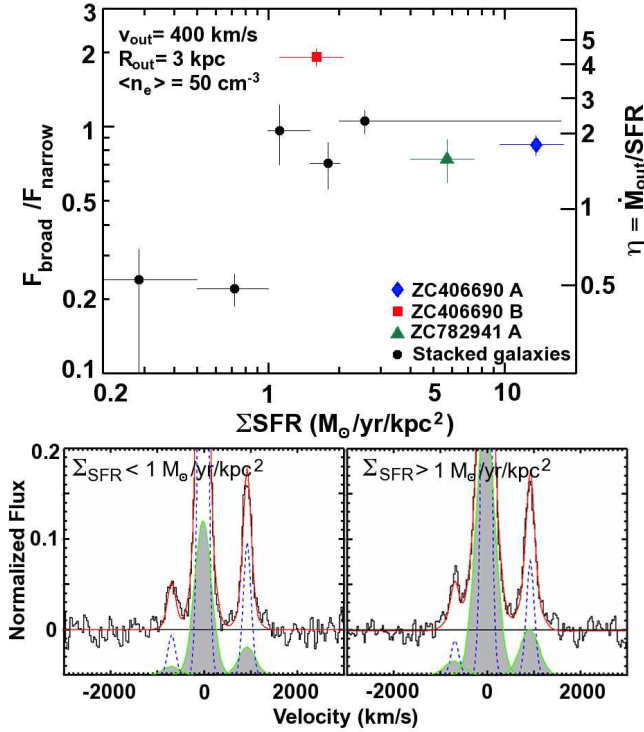


FIG. 2.— Dependence of the broad to narrow H α flux ratio on Σ_{SFR} . Above: Stacks in 5 star formation surface density bins with 5–8 galaxies each. The right vertical axis shows the corresponding mass loading with the model explained in the text and wind parameters listed in the figure. The black points are the stacked galaxies and the colored symbols are individual star-forming clumps. The horizontal error bars for the binned points represent the range in Σ_{SFR} for the galaxies in each bin. The vertical error bars represent the rms of the range in F_{broad}/F_{narrow} values achieved by varying the stacks (for the binned points) and the measurement error (for the clumps). Below: Co-added H α + [NII] spectra of low and high Σ_{SFR} bins with the data in black, the best fit shown in red, the narrow components shown in blue, and the broad components shown in green with grey shading.

assumed a mass outflow density of 100 cm^{-3} , based on two different outflow geometries and estimates of outflow density from local starburst galaxies (see e.g. Heckman et al. 1990). Thus we assume that these two values are upper and lower limits and take an average, resulting in a wind density of 50 cm^{-3} . Figure 3 shows the co-added spectrum along with the best fit.

A comparison of the narrow and broad [NII]/H α ratios (0.17 ± 0.017 and 0.31 ± 0.028 , respectively) with those of Newman et al. (2012) in the clump and wind regions of ZC406690 shows that the narrow [NII]/H α ratio is quite similar to the clump value and the broad ratio is very similar to that of the wind regions, which are affected by shocks. Therefore, not only does the broad [SII] ratio tell us about the density in the wind, but the broad [NII]/H α value provides further evidence that the broad component derives from outflows.

3.4. Mass-loading of High- z Galactic Outflows

We assume the simplified outflow model of Genzel et al. (2011) and Newman et al. (2012) for a warm ionized outflow with a radially constant outflow velocity and mass loss rate, to convert the F_{broad}/F_{narrow} ratio in Figure 2 into a mass-loading

factor $\eta \equiv \dot{M}_{out}/SFR$,

$$\dot{M}_{out} = M_w \times \frac{v_{out}}{R_{out}} = \frac{1.36 m_H}{\gamma_{H\alpha} n_e} \left(L_{H\alpha} \times \frac{F_{broad}}{F_{total}} \right) \frac{v_{out}}{R_{out}} \quad (1)$$

where \dot{M}_{out} is the mass outflow rate, M_w is the instantaneous mass in the outflow, v_{out} is the average velocity of the outflow, R_{out} is the radial extent, m_H is the atomic mass, $\gamma_{H\alpha}$ is the H α emissivity at $T_e = 10^4 \text{ K}$ ($\gamma_{H\alpha} = 3.56 \times 10^{-25} \text{ erg cm}^3 \text{ s}^{-1}$), n_e is the local electron density in the outflow, $L_{H\alpha}$ is the total extinction-corrected H α luminosity, and F_{broad}/F_{total} is the fraction of the total flux in the broad component. We assume $v_{out} = 400 \text{ km/s}$ (see section 4) and $R_{out} = 3 \text{ kpc}$. The latter is based on the spatial offset of outflowing gas from a massive star-forming clump described in Newman et al. (2012), and from the finding in section 3.1 that the broad emission is extended to several kpc from the galaxy center. The emission line based estimate is independent of the collimation of the outflow. We adopt $n_e = 50 \text{ cm}^{-3}$ as the average local electron density, derived in the previous section.

The inferred mass loading factors corresponding to the broad flux fraction are shown on the right-most y-axis in Figure 2. The mass-loading factors for galaxies below the Σ_{SFR} threshold are ~ 0.5 and above the threshold are ~ 2 , albeit with an overall absolute uncertainty of at least a factor of 3. Despite the uncertainties, a mass loading factor of 2 is consistent with observations of both local starbursts (Heckman et al. 1990; Veilleux et al. 2005; Chen et al. 2010) and high- z SFGs (Pettini et al. 2000; Weiner et al. 2009; Steidel et al. 2010; Genzel et al. 2011; Bouché et al. 2012), as well as theoretical predictions (Murray et al. 2005; Davé et al. 2011; Hopkins et al. 2012).

4. WHY DO THE OUTFLOWS DEPEND SO STRONGLY ON Σ_{SFR} ?

We propose that the strong dependence of η on Σ_{SFR} discussed in section 3.4 is mainly caused by the threshold that governs when star formation feedback can break out of the dense gas layer in the disk.

Following Ostriker & Shetty (2011) (see Equations 1 and 7), in a baryon dominated galactic disk in pressure equilibrium, the weight of the disk balances the pressure generated from star-formation feedback in the form of supernovae, stellar winds, HII regions, cosmic rays and radiation from the star-forming layer. If that pressure exceeds the weight of the disk, then a momentum-driven outflow is launched perpendicular to the galactic plane, with a threshold $\Sigma_{SFR} (M_\odot \text{ yr}^{-1} \text{ kpc}^{-2})$ of,

$$\Sigma_{SFR,th} = \frac{\pi G f_g}{2(P_{tot}/m_*)} \Sigma_d^2 = 0.9 \times \frac{f_{g,0.5} \times \Sigma_{d,500}^2}{(P_{tot}/m_*)_{1000}} \quad (2)$$

where G is the gravitational constant, (P_{tot}/m_*) is the characteristic total momentum injection per mass, Σ_d is the disk surface density, and f_g is the gas fraction, with fiducial values of 1000 km/s (Ostriker & Shetty 2011; Murray et al. 2005), $500 M_\odot \text{ pc}^{-2}$ (Erb et al. 2006; Förster Schreiber et al. 2009) and 0.5 (Tacconi et al. 2010; Daddi et al. 2010), respectively. Here, we have

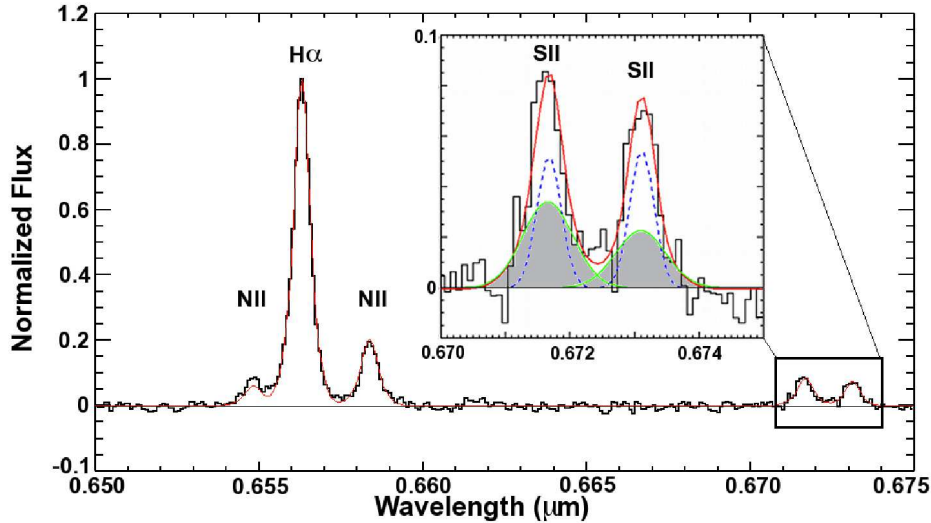


FIG. 3.— Co-added spectrum of 14 SFGs with [SII] detections that are free of OH contamination. The black line is the data, the red line is the best fit, and the green lines with grey shading (with FWHM = 407 km/s) and blue dashed lines (with FWHM = 197 km/s) (seen in the inset) are the broad and narrow Gaussian fits, respectively.

equated the weight of the gas above the disk (see: Ostriker & Shetty 2011, Equation 1, with an added dependency on f_{gas} since we only care about infalling gas) with the pressure from star formation feedback (see: Ostriker & Shetty 2011, Equation 7). This is similar to the Eddington limit of momentum driven winds (Murray et al. 2011), which gives $\Sigma_{SFR,threshold} \propto v_c^{5/2} R^{-2}$, where v_c is the circular velocity.

The wind has a total momentum outflow rate,

$$\dot{M}_w v_\infty \leq \left(\frac{P_{tot}}{m_*} \right) SFR \quad (3)$$

where v_∞ is the outflow velocity at large distances from the mid-plane, implying a mass-loading factor,

$$\eta = \frac{\dot{M}_w}{SFR} \leq \frac{(P_{tot}/m_*)}{v_\infty} = 2.5 \times \frac{(P_{tot}/m_*)_{1000}}{v_{\infty,400}} \quad (4)$$

with $v_{\infty,400}$ in units of 400 km/s. This velocity is motivated by the observed outflow velocities in both low- z and high- z SFGs (Pettini et al. 2000; Martin 2005; Veilleux et al. 2005; Weiner et al. 2009; Steidel et al. 2010; Genzel et al. 2011) as well as from this work. The adopted value of the characteristic momentum injection is chosen assuming P_{tot}/m_* from radiation pressure ~ 200 – 300 km/s (Ostriker & Shetty 2011) and that the direct momentum injection contributions of supernovae, stellar winds, HII regions and radiation pressure are all roughly comparable (Murray et al. 2005, 2010), giving a total (P_{tot}/m_*) of 1000 km/s. Here, we have assumed that energy-driven winds are unimportant and that the bulk of the ram pressure from SNe does not play a strong role until the gas has been lifted out of the disk (see: Murray et al. 2011).

This simple model predicts that for constant η the ability of an outflow to break out of the disk strongly depends on the star formation surface density, and this threshold value scales linearly with gas fraction and as the square of the disk surface density. Second, the mass

loading of galactic winds above breakout and the threshold star formation surface density for breakout both depend on (P_{tot}/m_*) . Thus, if one of these quantities can be determined for a galaxy of known properties, then the other can be predicted. The model also predicts that it is harder to launch a wind from a more massive galaxy (with larger v_c^4/R^2). This final prediction is also acquired by writing the threshold in terms of m_* by assuming (1) the $R_{1/2}$ - m_* relation of Ichikawa et al. (2012) ($R_{1/2} \sim m_*^{0.14}$), (2) the SFR- m_* relation for normal SFGs ($SFR = m_*^{0.7} \times ((1+z)/3.2)^{2.6}$) (Elbaz et al. 2007; Noeske et al. 2007) and (3) a constant gas depletion timescale ($t_{depl} = M_g/SFR \sim 6.4 \times 10^8$ yr, Tacconi et al. (2012)). We note that the Ichikawa et al. (2012) relation was derived using K band continuum emission, while our $R_{1/2}$ are derived using H α , so there may be some inconsistency. This gives an m_* threshold of $\sim \text{few} \times 10^{10} M_\odot$, such that it is easier for outflows to ‘break-out’ from galaxies below this threshold.

The first two predictions are met by the available data. For $z \sim 0$ normal SFGs with $f_g \sim 0.07$ and $\Sigma_d \sim 500 M_\odot \text{pc}^{-2}$ (Catinella et al. 2010), Equation 4 suggests a critical break-out star formation surface density of $\sim 0.1 M_\odot \text{yr}^{-1} \text{kpc}^{-2}$. And indeed, winds are only detected in compact star forming dwarfs and/or starbursts above $\sim 0.1 M_\odot \text{yr}^{-1} \text{kpc}^{-2}$ (Heckman et al. 1990; Veilleux et al. 2005; Chen et al. 2010), see also Murray et al. (2011). Mass loading factors for local galaxies with winds are estimated to be around 1 (Martin et al. 2012).

For the typical high- z SFGs presented in this paper ($f_g \sim 0.5$, $\Sigma_d \sim 500$ – $1000 M_\odot \text{pc}^{-2}$), Equation 2 suggests a breakout star formation surface density near or slightly above $1 M_\odot \text{yr}^{-1} \text{kpc}^{-2}$, in remarkable agreement with our findings in section 3.2 and Figure 2. Above this threshold, Equation 4 predicts a mass loading of ~ 2.5 , again in good agreement with our observations. We caution that our determination of the mass loading factor in the previous section is dependent on a simplified model with fairly uncertain parameters, yet the agreement is encouraging.

A positive correlation of η with Σ_{SFR} (which was also observed by Chen et al. (2010)) is possible evidence against the scenario in which winds are launched by the energy of hot supernovae bubbles, as in this case the shorter cooling time of the dense gas suggests $\eta \propto \Sigma_{SFR}^{-1/2}$ (Hopkins et al. 2012), and could support the momentum-driven wind model.

However, the third prediction of the simple model (massive galaxies are less efficient at driving winds) does not appear to be met by our data. For the SFGs in the ‘wind regime’ ($\Sigma_{SFR} > 1 \text{ M}_{\odot} \text{ yr}^{-1} \text{ kpc}^{-2}$) we do not see any significant variation of F_{broad}/F_{narrow} as a function of v_c , which is expected theoretically for momentum driven winds ($\eta \propto v_c^{-1}$, Murray et al. 2005; Oppenheimer & Davé 2006, 2008; Hopkins et al. 2012).

This finding as well as the approximate m_* independence of the observed F_{broad}/F_{narrow} ratio in our data surprisingly suggest that massive SFGs have mass loading factors that are similar to or higher than those of low mass SFGs. If so, the volume averaged outflow rate and metal enrichment of the circum-galactic/intergalactic medium at $z \sim 2$ may be dominated by massive galaxies just around the Schechter mass ($\log M_* \sim 10.65$, Peng et al. 2010). Indeed, with a slope α of the main-sequence of SFGs ($SFR \propto m_*^{\alpha}$) ~ 0.7 or higher, the SFR

(and thus the outflow rate, with constant η) increases faster with m_* than the volume density of SFGs decreases ($\Phi(m_*) \sim m_*^{-0.5}$, Peng et al. (2010)). We note that a massive galaxy dominance in the metal enrichment of the intracluster medium (ICM) is demanded by the fact that in clusters $\sim 2/3$ of the metal mass is contained in the ICM whereas only $\sim 1/3$ is still locked into stars and galaxies (Renzini 1997).

Further, the $z \sim 2$ m_* dependence of the mass-metallicity relation ($Z \sim m_*^{0.24}$, Erb et al. 2006) may be primarily driven by the larger (diluting) gas fractions in low m_* SFGs, besides these galaxies driving winds more effectively ($M_g/m_* = t_{depl} \times SFR/m_* \sim m_*^{-0.3}$). In addition, if high- m_* galaxies are indeed ejecting this much mass, we may have uncovered a mechanism contributing to the quenching of star formation near the Schechter mass (Peng et al. 2010).

We would like to thank the anonymous referee for a very thoughtful and useful review. We are grateful to Jerry Ostriker for a very valuable discussion on the wind breakout. SFN is supported by an NSF grfp grant. CM, AR, GZ and DV acknowledge partial support by the ASI grant ‘‘COFIS-Analisi Dati’’ and by the INAF grants ‘‘PRIN-2008’’ and ‘‘PRIN-2010’’.

REFERENCES

- Adelberger, K. L. et al. 2004, ApJ, 607, 226
 Bonnet, H. et al. 2004, Proc. SPIE, 5490, 130
 Bordoloi, R. et al. 2011, ApJ, 743, 10
 Bouché, N. et al. 2012, MNRAS, 3207
 Bruzual, G. & Charlot, S. 2003, MNRAS, 344, 1000
 Calzetti, D. et al. 2000, ApJ, 533, 682
 Catinella, B. et al. 2010, MNRAS, 403, 683
 Cecil, G., Bland-Hawthorn, J., Veilleux, S., & Filippenko, A. V. 2001, ApJ, 555, 338
 Chabrier, G. 2003, PASP, 115, 763
 Chen, Y.-M. et al. 2010, AJ, 140, 445
 Daddi, E. et al. 2010, ApJ, 714, L118
 Daddi, E. et al. 2004, ApJ, 600, L127
 Davé, R., Finlator, K., & Oppenheimer, B. D. 2011, MNRAS, 416, 1354
 Davies, R. et al. 2011, ApJ, 741, 69
 Davies, R. I. 2007, MNRAS, 375, 1099
 Eisenhauer, F. et al. 2003, Proc. SPIE, 4841, 1548
 Elbaz, D. et al. 2007, A&A, 468, 33
 Erb, D. K. et al. 2003, ApJ, 591, 101
 Erb, D. K. et al. 2006, ApJ, 646, 107
 Förster Schreiber, N. M. et al. 2009, ApJ, 706, 1364
 Förster Schreiber, N. M. et al. 2012, in prep.
 Genzel, R. et al. 2011, ApJ, 733, 101
 Heckman, T. M., Armus, L., & Miley, G. K. 1990, ApJS, 74, 833
 Hopkins, A. M. & Beacom, J. F. 2006, ApJ, 651, 142
 Hopkins, P. F., Quataert, E., & Murray, N. 2012, MNRAS, 421, 3522
 Ichikawa, T., Kajisawa, M., & Akhlaghi, M. 2012, MNRAS, 422, 1014
 Kennicutt, Jr., R. C. 1998, ApJ, 498, 541
 Komatsu, E. et al. 2011, ApJS, 192, 18
 Kornei, K. A. et al. 2012, ApJ, 758, 135
 Kurk, J. et al. 2009, A&A, 504, 331
 Law, D. R. et al. 2009, ApJ, 697, 2057
 Law, D. R. et al. 2012, ApJ, 759, 29
 Lilly, S. J. et al. 2009, ApJS, 184, 218
 Lilly, S. J. et al. 2007, ApJS, 172, 70
 Mancini, C. et al. 2011, ApJ, 743, 86
 Martin, C. L. 2005, ApJ, 621, 227
 Martin, C. L. et al. 2012, arXiv:1206.5552
 McCracken, H. J. et al. 2010, ApJ, 708, 202
 Murray, N., Ménard, B., & Thompson, T. A. 2011, ApJ, 735, 66
 Murray, N., Quataert, E., & Thompson, T. A. 2005, ApJ, 618, 569
 Murray, N., Quataert, E., & Thompson, T. A. 2010, ApJ, 709, 191
 Newman, S. F. et al. 2012, ApJ, 752, 111
 Noeske, K. G. et al. 2007, ApJ, 660, L43
 Oppenheimer, B. D. & Davé, R. 2006, MNRAS, 373, 1265
 Oppenheimer, B. D. & Davé, R. 2008, MNRAS, 387, 577
 Osterbrock, D. E. 1989, Astrophysics of gaseous nebulae and active galactic nuclei (University Science Books)
 Ostriker, E. C. & Shetty, R. 2011, ApJ, 731, 41
 Peng, Y.-j. et al. 2010, ApJ, 721, 193
 Pettini, M., Steidel, C. C., Adelberger, K. L., Dickinson, M., & Giavalisco, M. 2000, ApJ, 528, 96
 Renzini, A. 1997, ApJ, 488, 35
 Schreiber, J., Thatte, N., Eisenhauer, F., Tecza, M., Abuter, R., & Horrobin, M. 2004, in ASP Conf. Ser. 314, Astronomical Data Analysis Software and Systems (ADASS) XIII, ed. F. Ochsenbein, M. G. Allen, & D. Egret, 380
 Shapiro, K. L. et al. 2009, ApJ, 701, 955
 Shapley, A. E., Steidel, C. C., Pettini, M., & Adelberger, K. L. 2003, ApJ, 588, 65
 Steidel, C. C. et al. 2010, ApJ, 717, 289
 Steidel, C. C. et al. 2004, ApJ, 604, 534
 Tacconi, L. J. et al. 2010, Nature, 463, 781
 Tacconi, L. J. et al. 2012, in prep.
 Tremonti, C. A. et al. 2004, ApJ, 613, 898
 Veilleux, S., Cecil, G., & Bland-Hawthorn, J. 2005, ARA&A, 43, 769
 Veilleux, S., Cecil, G., Bland-Hawthorn, J., Tully, R. B., Filippenko, A. V., & Sargent, W. L. W. 1994, ApJ, 433, 48
 Weiner, B. J. et al. 2009, ApJ, 692, 187
 Westmoquette, M. S., Smith, L. J., Gallagher, J. S., & Exter, K. M. 2007, MNRAS, 381, 913